Adapting a Plant Tissue Model to Animal Development: Introducing Cell Sliding into VirtualLeaf

Wolff, H.B.; Davidson, L.A.; Merks, R.M.H.

Bulletin of Mathematical Biology (2019) 81:3322–3341
https://doi.org/10.1007/s11538-019-00599-9

Society for Mathematical Biology

SPECIAL ISSUE: MULTISCALE MODELING OF TISSUE GROWTH AND SHAPE

Adapting a Plant Tissue Model to Animal Development: Introducing Cell Sliding into VirtualLeaf

Henri B. Wolff[1,2,3] · **Lance A. Davidson**[2] · **Roeland M. H. Merks**[1,4,5]

Received: 14 June 2018 / Accepted: 11 March 2019 / Published online: 29 March 2019

Abstract

Cell-based, mathematical modeling of collective cell behavior has become a prominent tool in developmental biology. Cell-based models represent individual cells as single particles or as sets of interconnected particles and predict the collective cell behavior that follows from a set of interaction rules. In particular, vertex-based models are a popular tool for studying the mechanics of confluent, epithelial cell layers. They represent the junctions between three (or sometimes more) cells in confluent tissues as point particles, connected using structural elements that represent the cell boundaries. A disadvantage of these models is that cell–cell interfaces are represented as straight lines. This is a suitable simplification for epithelial tissues, where the interfaces are typically under tension, but this simplification may not be appropriate for mesenchymal tissues or tissues that are under compression, such that the cell–cell boundaries can buckle. In this paper, we introduce a variant of VMs in which this and two other limitations of VMs have been resolved. The new model can also be seen as on off-the-lattice generalization of the Cellular Potts Model. It is an extension of the open-source package VirtualLeaf, which was initially developed to simulate plant tissue morphogenesis where cells do not move relative to one another. The present extension

This work was cofinanced by the Netherlands Consortium for Systems Biology (NCSB; 2008–2013), which was part of the Netherlands Genomics Initiative/Netherlands Organisation for Scientific Research (HBW and RMHM). This work was also part of the research program Inovational Research Incentives Scheme Vidi Cross-divisional 2010 ALW with Project No. 864.10.009 and Vici 2017 ENW with Project No. 865.17.004 to RMHM, which are (partly) financed by the Netherlands Organization for Scientific Research (NWO). The simulations were carried out on the Dutch national e-infrastructure with the support of SURF Cooperative (www.surfsara.nl, Lisa). Support for LAD and partial support for HBW were provided by grants from the National Institutes of Health (NIH R01 HD044750, R21 ES019259 and R01 HL136566) and the National Science Foundation (NSF CMMI-1100515). Any opinions, findings, and conclusions or recommendations expressed in this material are those of the authors and do not necessarily reflect the views of the NSF or the NIH.

Electronic supplementary material The online version of this article (https://doi.org/10.1007/s11538-019-00599-9) contains supplementary material, which is available to authorized users.

Extended author information available on the last page of the article

of VirtualLeaf introduces a new rule for cell–cell shear or sliding, from which cell rearrangement (T1) and cell extrusion (T2) transitions emerge naturally, allowing the application of VirtualLeaf to problems of animal development. We show that the updated VirtualLeaf yields different results than the traditional vertex-based models for differential adhesion-driven cell sorting and for the neighborhood topology of soft cellular networks.

Keywords Cell-based modeling · Vertex-based model · Cellular Potts Model · Developmental biology · Epithelial tissues · Junction remodeling · Cell sorting · Bubbly vertex model · Cell rearrangement · Epithelial morphogenesis

1 Introduction

How cells form tissues, organs, and organisms remains one of the most intriguing and most central questions of biology. Recent theoretical approaches to study collective cell behavior are taking a prominent role in addressing these questions. Theoretical approaches provide deeper intuition about processes that typically are unfamiliar to the researchers by testing the physical plausibility of speculative hypotheses or by making predictions that can be tested experimentally. Theory can aid the analysis of data-rich time-lapse images of cell movements during development (Brodland et al. 2014; Merkel and Manning 2017) by simulating how the behavior of individual cells might lead to collective behavior and how collective movements might influence individual cell behaviors. To support theoretical analysis of tissue formation, a large range of mathematical methods have been proposed. These range from systems of partial differential equations models (see, e.g,. Keller and Segel 1970, 1971; Painter et al. 2015) to discrete methods that describe dense multicellular structures as interacting particle systems (see, e.g., Glazier and Graner 1993; Graner and Glazier 1992; Newman 2005; Sozinova et al. 2006; Voss-Böhme and Deutsch 2010; Woods et al. 2014; Smeets et al. 2016; Barton et al. 2017; Ghaffarizadeh et al. 2018 and Liedekerke et al. 2015 for review).

In contrast to continuum models, such so-called cell-based (Merks and Glazier 2005; Merks 2015) or single-cell-based methods (Anderson et al. 2007) have the disadvantage that formal dynamical analyses are impossible except in relatively simple cases (Voss-Böhme and Deutsch 2010). Nevertheless, in many biological applications cell-based models are preferred as they can incorporate ‘biological rules’ that reflect more physiologically realistic biology than can be achieved easily in continuum methods. For example, Odell et al. (1981) posed a calcium sensitive feedback system to spread a contraction wave. As developmental biologists adopt biophysical methods and borrow principles of control theory to explain tissue formation, simulations will need to capture interactions between multiple cell types and the diverse forms of cell–cell communication those interactions encode (Lander 2007). Models will further need to integrate structural, mechanical, and biochemical cues with downstream effectors of morphogenesis such as cell division, cell death events, and cell differentiation events (Maree and Hogeweg 2002; Hester et al. 2011; Boas et al. 2015; Palm et al. 2016). Cell-based simulation methods provide a rich framework to study

multiscale phenomena such as these, in that they simulate the dynamics of the cell and the tissue as a whole, while subcellular dynamics can be naturally integrated, such as gene regulation, secretion of signaling molecules, the dynamics of the cytoskeleton, and electrophysiological mechanisms (Boas and Merks 2014; Belmonte et al. 2016; Sluka et al. 2016; Kudryashova et al. 2017). Thus, cell-based modeling approaches enable integration of the physics of collective cell behavior with diverse modes of subcellular biological regulation.

A large range of cell-based modeling techniques are available; they can be roughly classified into single-particle and multiparticle methods, and lattice-based and off-lattice techniques (Merks 2015). Single-particle techniques are efficient computationally and have found wide application, but they also have limitations. For example, cell shape can affect the outcome of cell–cell interactions: cells that mutually attract one another via a chemoattractant form network-like structures if they are elongated, while they form separate 'islands' if they are rounded (Merks et al. 2006). Also, it can be important that subcellular compartments interact with their local environment relatively independently from one another. For example, contact inhibition of cellular protrusions can promote directional migration of neural crest cells (Carmona-Fontaine et al. 2008). Although it is possible to simulate such problems using single-particle-based methods [see, e.g., Palachanis et al. (2015) for effects of cell shape in vascular patterning, Woods et al. (2014) for neural crest cell migration; and for cell sorting see, e.g., Sulsky et al. (1984); Graner and Sawada (1993); Osborne et al. (2017)], multiparticle methods allow for a large flexibility in cell shape that is more directly related to cell shapes acquired from time-lapse microscopy. Multiparticle methods are also better suited for the simulation of local mechanisms responsible for collective behavior (e.g., contact inhibition Woods et al. 2014), as they make it possible to reduce cell-level assumptions to subcellular mechanisms.

Two widely used multiparticle techniques for cell-based modeling include the Cellular Potts Model (CPM) and the vertex-based model (VM). The CPM represents cells as (usually connected) domains of lattice sites on a regular lattice. Cells move on the lattice by randomly extending or retracting their domain to adjacent lattice sites, according to a Hamiltonian energy function that describes the contractile and viscoelastic structures that form each cell, the physical adhesive interactions between cells, and in some cases, extracellular materials. Alternatively, structural elements have been used to describe the cell boundaries and cross-linking elements for the cell interior (Odell et al. 1981). A simplified version of this model is the vertex-based model (VM) (Weliky and Oster 1990; Honda et al. 1983; Staple et al. 2010). These represent the junctions between three (or sometimes more) cells in confluent tissues as point particles, connected using structural elements that represent the cell boundaries. Where the CPM defines tissues as assemblages of cells with individual cells represented as collections of adjacent lattice sites, VM describes the tissue as a polygonal tessellation of junctionally connected cells with each cell represented by a series of nodes representing three-cell junctions.

In principle, CPM and VM are equivalent. Like cells in CPMs, the dynamic movements of cells in VMs are driven by the physical properties of cell–cell interfaces, which are governed by a Hamiltonian function that usually includes interfacial tensions, cell adhesion, and cell area constraints. The parameters of CPM or VM can

often be rescaled such that the model can be run in the other formalism (Magno et al. 2015). However, some cases can arise where the two modeling frameworks cannot be interconverted (Osborne et al. 2017). For instance, because the string-like elastic elements in their basic formulation describe cell–cell interfaces and require all cells to be interconnected, VMs are unsuitable for non-confluent tissues. In this paper, we discuss further limitations of traditional VMs including (a) description of cell–cell interfaces as straight lines, (b) separation of membrane fluctuations and model dynamics, and (c) algorithms that represent cell neighbor changes with rule-based T1 and T2 transitions.

In this paper, we introduce a variant of the VM in which these three limitations have been resolved. The model is an extension of the open-source package VirtualLeaf (Merks et al. 2011; Merks and Guravage 2012) (also see the re-engineered derivative *Virtual Plant Tissue*; De Vos et al. 2017), which was initially developed to simulate plant tissue morphogenesis where cells do not move relative to one another. VirtualLeaf differs from traditional VMs in that (a) cell interfaces are represented by multiple nodes that allow membrane fluctuations; (b) tissue topology changes exclusively through cell division with no T1 or T2 transitions; and (c) tissue dynamics are advanced used a Metropolis algorithm that incorporates membrane fluctuations. The present extension of VirtualLeaf introduces a new rule for cell–cell shear or sliding, from which T1 and T2 transitions emerge naturally, allowing the application of VirtualLeaf to problems of animal development.

We will discuss two cases for which the updated VirtualLeaf yields different results than traditional VM. First, we discuss simulations of differential adhesion-driven cell sorting and show that the new update rule for cell sliding facilitates complete cell sorting. We will then turn our attention to epithelial dynamics and discuss cases for which the flexibility of cell membranes affects the neighborhood topology of soft networks (Farhadifar et al. 2007).

2 Methods

VirtualLeaf represents confluent tissues in two dimensions as a set of interconnected polygonal cells. A cell $C_i = \{V_i, E_i, \alpha_i\}$ is defined by a set of n vertices, $V_i = \{\mathbf{v}_1 \ldots \mathbf{v}_n\}$ that are connected by m edges, $E_i = \{\mathbf{e}_1 \ldots \mathbf{e}_m\}$, and a set of cell attributes, α_i. Adjacent cells share the same vertices and edges. Thus, the tissue $T = \{C, V, E\}$ is defined by the set of all cells in the tissue, C, and by all vertices in the tissue, $V = \bigcup_{i \in T} V_i$ and all edges, $E = \bigcup_{i \in T} E_i$ (Fig 1a). A Hamiltonian function, H, describes the balance of passive, mechanical forces in the tissue, including adhesive forces between cells, membrane tensions, and expansive cellular forces. The exact form of the Hamiltonian differs between models; in its simplest form (Merks et al. 2011) it includes a volume conservation term to resist compression of the cells and a line tension term to resist expansion of the membranes,

$$H = \lambda_A \sum_{c \in C} (A(c) - A_T(c))^2 + \lambda_M \sum_{\mathbf{e} \in E} (\|\mathbf{e}\| - L_T)^2 . \quad (1)$$

The first term on the right-hand side (RHS) is the volume conservation term. Here $A_T(c) \in \alpha_c$ is the resting area of cell c, *i.e.*, the area it would take up in the absence of counteracting compressive or expansive forces, $A(c)$, the actual area of cell c, and λ_A is a Lagrange multiplier. The second RHS term gives the energy of the cell boundary, which is represented as a set of connected springs of rest length L_T. The sum runs over the edges e taken from E, the set of all edges in the simulation, and λ_M is a Lagrange multiplier.

We update the model using Metropolis dynamics: We iteratively select a random node $\mathbf{v}_i$ and attempt to move it to a randomly chosen new position $\mathbf{v}_i' = \mathbf{v}_i + \boldsymbol{\xi}\Delta x$, with $\boldsymbol{\xi} \in \{[-1/2, 1/2], [-1/2, 1/2]\}$, i.e., a random vector chosen uniformly from a square of size 1×1 centered at $(0, 0)$, and Δx the step size. The algorithm calculates the change of the Hamiltonian resulting from the attempt, ΔH, and accepts the move if $\Delta H < 0$. To keep the system from settling into local minima and to mimic active, random cell motility, we also accept moves increasing the Hamiltonian $\Delta H > 0$ with Boltzmann probability $P(\Delta H) = \exp(-\Delta H/T)$, with the Boltzmann temperature, T, setting the amount of random cell motility or 'noise' added in this way.

The key novelty that makes the model applicable to animal tissues is that here we allow cells to move through the tissue. To this end, we introduce a *sliding operator* to further reduce the Hamiltonian (Fig. 1c). The sliding operator allows a cell edge that is part of a tricellular or higher order junction to 'hop' to another vertex. For example an edge connecting nodes $\mathbf{v}_1$ and $\mathbf{v}_2$ can be moved to connect nodes $\mathbf{v}_2$ and $\mathbf{v}_3$. Similar to the regular moves, a slide is accepted with probability $P(\Delta H) = \{1, \Delta H < 0; \exp(-\Delta H/T), \Delta H > 0\}$.

A single Monte Carlo Step (MCS) involves cycling over all nodes v in random order. For each node, we first attempt to move it. If the node is of order 3 or higher, we also try to slide it (see flowchart in Fig. 1f). After completion of one MCS, the descriptions of the cell membranes are refined if necessary, so as to keep an approximately even distribution of edge lengths. To do so, all edges $\mathbf{e} \in E$ whose length exceeds a threshold, $\|\mathbf{e}\| > l_{\max}$, are split into two by inserting a new vertex in the middle. Similarly, if $\|\mathbf{e}\| < l_{\min}$, the edge is deleted from the tissue, replacing the two vertices and their connections for a new, fused vertex containing the connections of the two original vertices combined.

Independent of this Hamiltonian description of cell mechanics and cell motility, additional rules motivated by the biological problem can be included, including cell growth, cell division, and subcellular models describing the genetic or metabolic networks regulating cell behavior using differential equations (Merks et al. 2011). If the additional rules can be safely assumed to run at a much slower rate than the cellular mechanics, we make a quasi-steady state assumption for the cellular mechanics: First, we iterate the Metropolis dynamics until the Hamiltonian has practically stabilized, that is, if $\Delta H/\Delta t < \epsilon$, with ϵ a small number; then, we apply the additional rules for a number of time steps. In other models (i.e., the cell sorting model), the Metropolis algorithm describes a kinetic mechanism that does not stabilize within the course of a simulation. In those cases, we apply an operator splitting approach in which the Monte Carlo steps are alternated with steps of the additional rules.

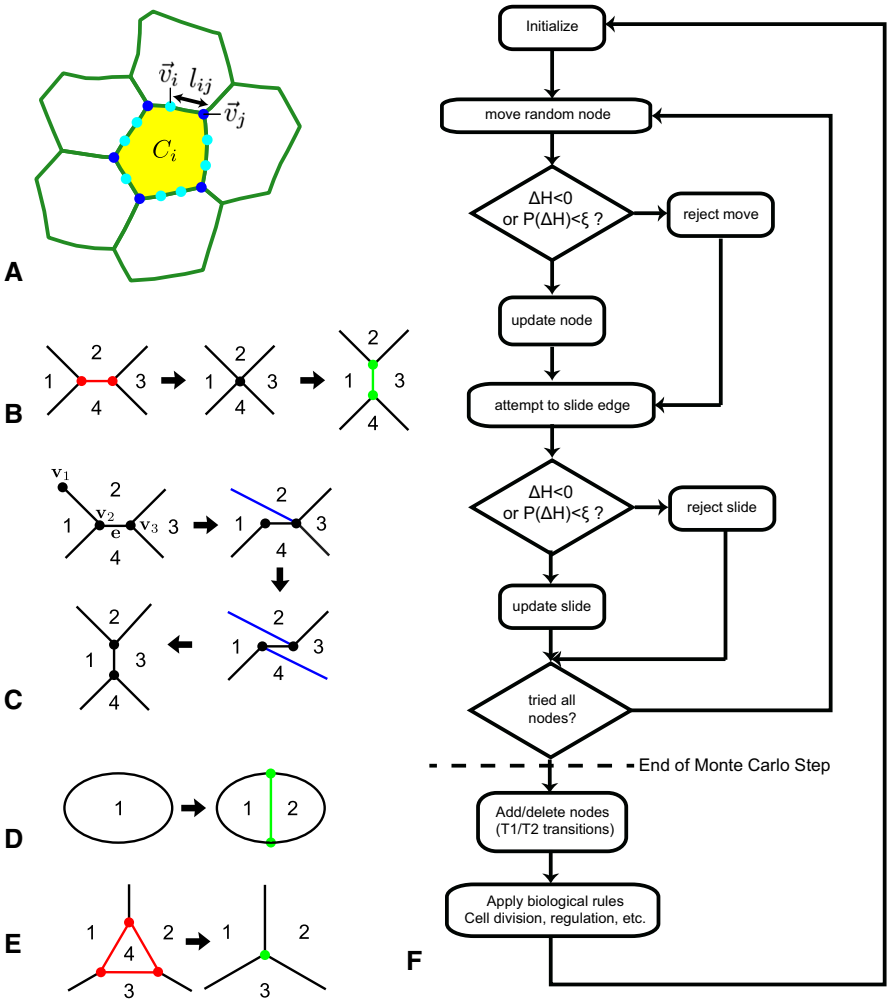

Fig. 1 Overview of the cell-based model. **a** Polygonal representation of a collection of cells. Cell C_i consists of edges (green) l_{ij} connected by nodes $\mathbf{v}_i$ and $\mathbf{v}_j$. Nodes that connect three or more cells are shown in dark blue. The 2 connected nodes (shown in light blue) account for membrane flexibility. **b–e** Topological rearrangements of vertices and edges. Numbers represent cells. New vertices and edges are green, and red vertices and edges are to be removed. Blue edges are moved by sliding. **b** Traditional approach through T1 transitions: One edge is added and one edge is removed; **c** Novel approach through slide events having the same topological effect as the T1 transition shown in (**b**); **d** Cell division; **e** T2 transition: A cell is removed from the tissue and replaced with a tricellular junction; **f** Flow chart of an extended VirtualLeaf simulation. During a Monte Carlo step, VirtualLeaf attempts to move and slide all nodes once in a random order. After one such loop, the network is rearranged, and 'biological rules' are applied (Color figure online)

3 Results

We validate the model extensions by looking at two classical problems: (a) differential adhesion cell sorting (Glazier and Graner 1993; Graner and Glazier 1992) and (b) cell packing in epithelial monolayers (Farhadifar et al. 2007). VirtualLeaf provides new insight into both problems.

3.1 Cell Sorting

Classic experiments by Holtfreter (reviewed in Steinberg 1996) have shown that cells of different embryonic tissues can phase separate. A number of closely related hypotheses have been proposed to explain this phenomenon. Steinberg (1963, 2007) has proposed the differential adhesion hypothesis. In this view, cell sorting is due to the interplay of differential adhesion and random cell motility, which progressively replaces weaker intercellular adhesions for stronger adhesions. In addition to differential adhesion, contraction of the cortical cytoskeleton contributes to the equilibrium configurations of mixed cell aggregates (Krieg et al. 2008), leading to the differential surface contraction (Harris 1976) aka differential interfacial tension (Brodland 2002) hypothesis.

Because of its importance for biological development and the possibility to predict the configuration corresponding with the energy minimum from the differential interfacial energies (Steinberg 1963), cell sorting has become a key benchmark problem for cell-based modeling methodology. Cell sorting has been reproduced in a practically all available cell-based models, including cellular automata (Antonelli et al. 1973), vertex-based models (Hutson et al. 2008), center-based models (Graner and Sawada 1993), and the Cellular Potts Model (Graner and Glazier 1992; Glazier and Graner 1993), but small differences are observed (Osborne et al. 2017): The kinetics of cell sorting differs between cell-based modeling methods as well as the extent to which the simulation gets trapped into local minima. Also, methodology relying on single particles to represent a cell may require unrealistically long interaction lengths or unrealistic cell motility models to achieve complete cell sorting (Osborne et al. 2017)

Following previous Cellular Potts and vertex-based approaches (Graner and Glazier 1992; Glazier and Graner 1993; Hutson et al. 2008), we assume that cell motility is governed by volume conservation and an adhesion energy defined at all cell–cell and cell–medium boundaries,

$$H = \lambda_A \sum_{c \in C} \left(A(c) - A_T(c)\right)^2 + \sum_{\mathbf{e} \in E} J\left(\mathbf{e} \rightarrow L, \mathbf{e} \rightarrow R\right) \|\mathbf{e}\| \tag{2}$$

with $A(c)$ and $A_T(c)$ the actual area and resting areas of the cells. The adhesion energy is a sum over all edges $\mathbf{e} \in E$ in the tissue, with parameter $J(\mathbf{e} \rightarrow L, \mathbf{e} \rightarrow R)$ the adhesion energy per unit cell-cell interface separating the cell at the left (L) and the cell at the right (R) of the interface, where one cell can be the medium.

3.1.1 Sliding Operator Enables Complete Cell Sorting

Figure 2a–c and Videos S1–S3 show the simulation results for three typical settings of the adhesion parameter J. The simulations are initiated with a configuration of 20×20 cells of size 10×10, with mixed or segregated cell type assignments as shown in the first column of Fig. 2. The target area is set equal to the initial area, at $A_T = 100$. The step size for the Monte Carlo algorithm is $\Delta x = 0.5$, $l_{\min} = 6$, and $l_{\max} = 8$. For these parameter settings, the nodes are moved randomly over a square of side $1/20$ of that of the initial length of the cell–cell interfaces, and one cell–cell interface consists typically of one to two edges, such that sliding moves occur over half to a full cell–cell interface.

In Fig. 2a, the heterotypic adhesion, i.e., the adhesion between green and red cells, is stronger than the homotypic adhesion, i.e., $J(\text{green, green}) = J(\text{red, red}) > J(\text{red, green})$. The model evolves toward a checkerboard configuration, which maximizes the contact area between red and green cells. Figure 2b, c shows example simulations for which the homotypic adhesion is stronger than the heterotypic adhesion, that is, $J(\text{green, green}) = J(\text{red, red}) < J(\text{red, green})$. In addition, in Fig. 2b the adhesion of the green cells with the surrounding medium is stronger than that of the red cells, i.e., $J(\text{green, ECM}) < J(\text{red, ECM})$. Cell sorting requires stochastic boundary movement; at $T = 0$ no energetically unfavorable moves are accepted, and the configuration gets stuck at the initial condition, whereas cell sorting is accelerated at higher temperatures (Fig. 2e). Altogether, in analogy with the Cellular Potts Model (Graner and Glazier 1992; Glazier and Graner 1993), the extended VirtualLeaf reproduces the key phenomena related to differential adhesion-driven cell rearrangement: cell sorting, checkerboard pattern formation, and engulfment.

In order to represent cell rearrangements, previous vertex-based simulations applied a rule-based T1 transitions. In these simulations, the T1 transition rearranges four adjacent cells as shown in Fig. 1b. The rule-based T1 transition is initiated if the length of an intercellular interface, i.e., an edge $\mathbf{e}$ connecting a 3-connected node v_1 with a second node v_2, drops below a threshold, $\|\mathbf{e}\| < \theta_{\text{T1}}$. The T1 transition then deletes $\mathbf{e}$ by fusing v_1 and v_2 and generates a new edge, $\mathbf{e}_\perp$, perpendicular to $\mathbf{e}$. In the absence of noise terms, vertex-based models based on such rule-based T1 transitions generally cannot achieve complete cell sorting, except in specific three-dimensional cases where almost complete cell sorting can be achieved (Hutson et al. 2008).

In the extended VirtualLeaf, T1 transitions are represented by a combination of two sliding moves, where both moves are driven by the Hamiltonian (Fig. 1c). As a first test of the extent to which the sliding operator changes the kinetics of cell sorting, in a second set of simulations we replaced it for rule-based T1 transitions. Figure 2d and Video S4 show a cell sorting experiment with only rule-based T1 transitions and a cellular temperature of $T = 10$, the same cellular temperature as that used in Fig. 2c. Without the sliding operator, cell sorting proceeds well over short times, with small clusters of green and red cells forming, but cell sorting remains incomplete. We have currently not investigated the causes of this in detail, but a potential factor is that the sliding operator is fully integrated in the energy minimization processes, in contrast to the rule-based treatment of T1 transitions. Also changing the threshold for rule-based T1 transitions, currently set at $\theta_{\text{T1}} = \Delta x/2 = 0.25$, will likely speed up cell sorting.

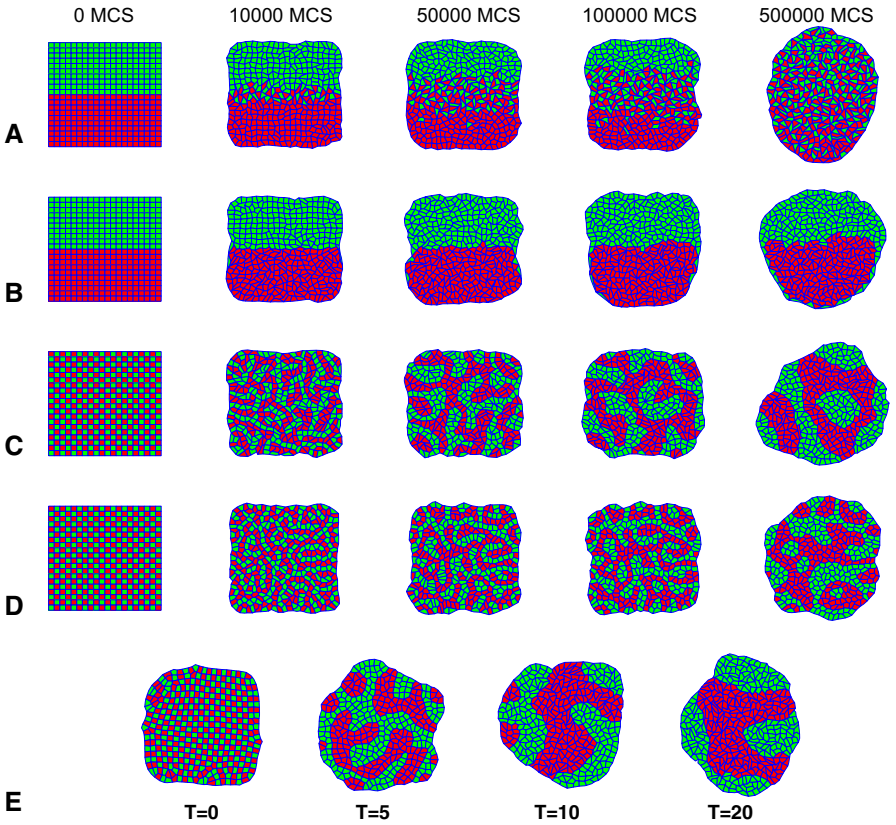

Fig. 2 Differential adhesion-driven cell rearrangement in the VirtualLeaf. Initial condition: 200 green and 200 red cells of $A_T = A(0) = 100$, as shown in first column, $l_{\min} = 6$, $l_{\max} = 8$, $\Delta x = 0.5$; $T = 10$ in (**a**–**d**): **a** cell mixing (J(green, green) $= J$(red, red) $= 20$, J(red, green) $= 10$, J(cell, medium) $= 30$), **b** engulfment (J(green, green) $= 20$, J(red, red) $= 10$, J(red, green) $= 20$, J(green, medium) $= 20$, J(red, medium) $= 40$); **c** cell sorting (J(green, green) $= 20$, J(red, red) $= 10$, J(red, green) $= 30$, J(cell, medium) $= 30$); **d** incomplete cell sorting with only T1 transitions with parameters as in (**c**) with $\theta_{\mathrm{T1}} = 0.25$; **e** configurations of cell sorting experiments at 500.000 MCS with increasing values of intrinsic motility (T) with parameters as in **c**. Simulation time is expressed in Monte Carlo Steps (MCS) (Color figure online)

We will leave a full analysis of the sliding operator relative to the rule-based treatment of T1 transitions to future work.

3.1.2 Differential Cortical Tension

As an experimental test of the differential adhesion hypothesis, Krieg and coworkers (Krieg et al. 2008) have measured the adhesive forces between induced germline progenitor cells from early zebrafish embryos. The heterotypic adhesion forces between induced endodermal, mesodermal, and ectodermal cells were approximately equal, whereas the homotypic adhesion forces differed between germ layers. Mesodermal cells adhered most strongly to one another, followed by endodermal cells, and ecto-

dermal cells had the weakest adhesive forces to one another. Based on these data, the authors estimated relative values of the adhesion parameters, J, in a Cellular Potts Model. Strikingly, in the Zebrafish germline progenitor aggregates the least coherent ectodermal cells sorted to the middle of the cellular aggregates. This finding contradicts the differential adhesion hypothesis (DAH), which predicts that the least cohesive cells move to the aggregate's periphery, see, e.g., the CPM (Graner and Glazier 1992) and our own simulations (Fig. 3, top-left to bottom-right diagonal). Krieg and coworkers demonstrated that the contradictory prediction can be attributed to differential cortical tension (DCT), an alternative to DAH (Harris 1976), with the highest cortical tension occurring at cell–medium interfaces. To implicitly incorporate cortical tension effects into the Cellular Potts Model, Krieg and coworkers reinterpreted the CPM such that a high value of J corresponded with a high interfacial tension.

To test if VirtualLeaf could represent both DAH and DCT explicitly in the same model framework, we modified the Hamiltonian (Eq. 2) to add a cell-dependent cortical tension term that is only active at the tissue boundaries. The new Hamiltonian becomes

$$H = \lambda_A \sum_{c \in C} \left(A(c) - A_T(c)\right)^2 + \sum_{\mathbf{e} \in E} J\left(\mathbf{e} \to L, \mathbf{e} \to R\right) \|\mathbf{e}\| + \lambda_{\text{cortical}} \sum_{\{c \in C | c \cap \partial C\}} \left(P(c) - P_T(c)\right)^2 \tag{3}$$

with ∂C, the boundary of the tissue, $\lambda_{\text{cortical}}$, a parameter and $P_T(c)$ a cell type- specific target perimeter. $P(c) = \sum_{\mathbf{e} \in (c \to E)} \|\mathbf{e}\|$ is the perimeter of cell c, and $P_T(c)$, a target perimeter. Note that the cortical tension term was only applied at the cell–medium interfaces, which would be equivalent to setting $\lambda_{\text{cortical}} = 0$ at cell–cell interfaces. The adhesion parameters were set such that $J(r, r) < J(g, g) < J(g, r)$, i.e., red cells are more coherent than green cells, and red–green interfaces are energetically unfavorable. We have also assumed increased line tension at the boundary of the cell aggregate due to myosin activity (Krieg et al. 2008), by setting $J(l, M) = 0$ and $J(d, M) = 0$, but this has little effect on the results.

Figure 3 shows a parameter study of this model. If the two cells have equal cortical tension at the boundary of the aggregate (top-left to bottom-right diagonal and Videos S5 and S6), the coherent red cells sort to the center, as expected in the absence of additional assumptions. The sorting order is reversed if $P_T(r) > P_T(g)$, thus reducing the cortical tension of red cells relative to that of the green cells (Fig. 3, upright corner and Video S7).

3.2 Epithelial Cell Packing

The structure of multicellular tissues and the shape of the constituent cells are driven by the interplay of cell division, cell growth, intercellular frictional forces, and global tissue mechanics. Epithelial tissues of plants (Kim et al. 2014) and of animals (Farhadifar et al. 2007) can be represented by two-dimensional tessellations and are, therefore, a popular model system for studying morphogenesis and emergence of tissue form (Lewis 1926). In particular, the number of neighbors in many epithelial tissues shows a characteristic distribution: Hexagonal cells are the most frequent, followed by pen-

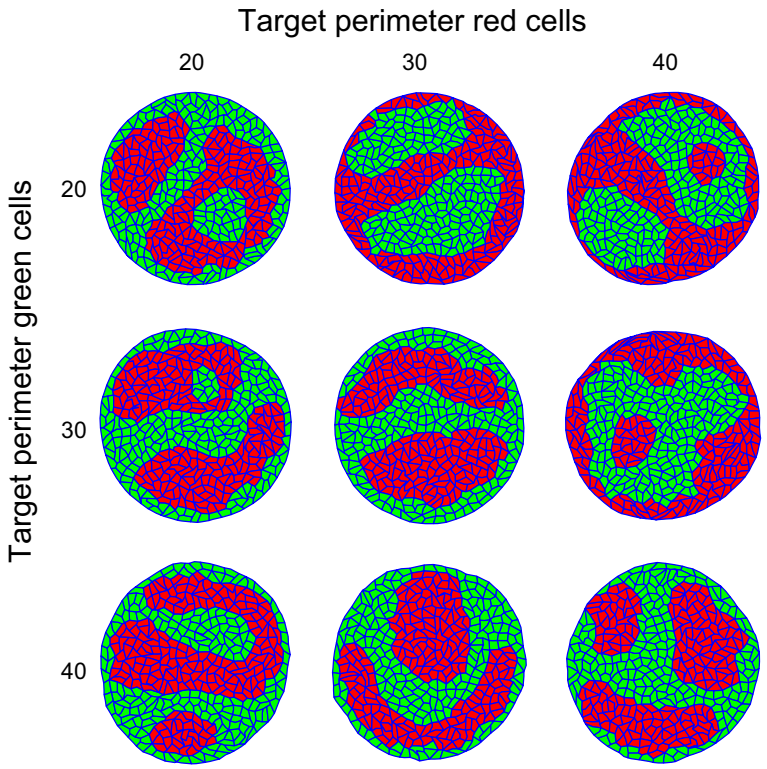

Fig. 3 Parameter study of interface-specific cortical tension. Simulations with cell type-specific cortical tension applied only at cell–medium interfaces with the target perimeter $P_T(c)$ equal to 20, 30 and 40 as indicated in the axis labels. All other parameters remain unchanged (see Supporting Text S1). This figure shows the tissues after a simulation of 500,000 MCS (Color figure online)

tagonal and heptagonal cells. Although the experimentally observed distribution can arise due to random cell division alone (Gibson et al. 2006), the biophysics of cell packing, i.e., programs of cell rearrangement and patterning of interfacial tensions, allows tissues to assume alternative, often narrower, i.e., more hexagonal neighbor distributions (Farhadifar et al. 2007). In the absence of cell rearrangements (as, e.g., in plant tissues), mathematical simulations have shown that cells must divide over the center of mass and the division plane must follow shortest paths, thus forming equally sized, symmetrically shaped daughter cells (Sahlin and Jönsson 2010).

3.2.1 VirtualLeaf can Reproduce Key Features of Epithelial Cell Packing

To see if our model, in particular the flexible cell membranes and the sliding operator, could lead to different predictions for epithelial tissues, we here focus on the results described by Farhadifar et al. (2007) using the model implementation detailed in Staple et al. (2010). Their vertex-based model uses a Hamiltonian of the form,

$$H = \lambda_A \sum_{c \in C} (A(c) - A_T(c))^2 + \sum_{\mathbf{e} \in E} J \|\mathbf{e}\| + \lambda_{\text{cortical}} \sum_{c \in C} (P(c) - P_T(c))^2 , \quad (4)$$

with $P_T(c) = 0$ and $J = J(\mathbf{e} \rightarrow L, \mathbf{e} \rightarrow R)$ the same for all cell interfaces. In the absence of cell division, in this model two distinctive equilibrium cell shape patterns or 'ground states' can emerge depending on the parameters. For positive line tension, $J > 0$, or negative line tension, $J < 0$, with a sufficient high contractility, $\lambda_{\text{cortical}}$, the global energy minimum in the absence of cell divisions (ground state) of the vertex model is a regular, hexagonal tessellation with cellular areas smaller than the target area. The hexagonal tessellation resists compression, expansion, or shearing. The alternative global minimum is a 'soft network,' which occurs at negative line tensions combined with no, or relatively low contractility. The soft network is characterized by many, alternative irregular tessellations of equal pattern energy, with cellular areas equal to the target area. This soft-to-stiff transition is thought to reflect a soft matter phase transition that accompanies jamming of granular materials (Atia et al. 2018; Tlili et al. 2018; Bi et al. 2015, 2016).

Farhadifar et al. (2007) have shown that the cell packing deviates from these global equilibria if cell division is introduced. The authors picked one cell at random, doubled its target area, and relaxed the cellular configuration to the nearest equilibrium using a conjugate gradient method. They then divided the cell over a randomly oriented axis passing through the cell centroid, after which they relaxed the configuration again to its nearest equilibrium. This procedure was repeated until the tissue consisted of 10,000 cells, after which the topology of the tissue was examined.

To determine if our simulation methods could reproduce these results, we used a vertex-based special case of VirtualLeaf, in which there were no 2-connected nodes, i.e., the cell-cell interfaces could not buckle and topological changes occurred through rule-based T1 and T2 transitions. We replicated Farhadifar's cell division algorithm with only minor modifications. We picked one cell at random, slowly increased its target area, and relaxed the tissue to steady state using the Metropolis algorithm. Once the actual area of this cell exceeded twice the target area of the other cells, we let the cell divide over a randomly oriented axis passing through the cell centroid and assigned the original target area to the daughter cells, and the procedure was repeated. Our simulations (Fig. 4a and Videos S8–S10) agree visually with the three cases reported previously (Farhadifar et al. 2007) and illustrate the key results of these simulations, displayed upon the ground state diagram by Farhadifar et al. (2007). Our vertex-based model replicates a typical 'stiff' network (Case I), located in the parameter region with a hexagonal ground state, producing cells of approximately uniform size. Furthermore, our model can replicate the outcome of cells with a higher cortical tension (Case II) producing cells with more variable areas and a tessellation that contains large polygons with nine sides or over. Lastly, our model can recapitulate the 'soft network' or ground state (Case III) where cells evolve irregular shapes equal to the target area.

After eight rounds of cell division, the distribution of polygon classes (P_n, the fraction of polygons in the final tissue with n sides) in Case I agree, with only minor differences, with those reported in Farhadifar et al. (2007) (red bars in Fig. 4c). Both models reveal pentagon and hexagon-shaped cells dominate at $P_5 \approx 0.3$ and $P_6 \approx 0.3$ while heptagons are slightly less frequent at $P_7 \approx 0.2$, and tetragons and octagons are present at frequencies of $P_4 \approx P_8 \approx 0.1$. Our model also has qualitative agreement in Case II and Case III with those reported for the vertex model although our model generated fewer 3-, 4-, 8-, and 9-sided cells. This difference can likely be attributed

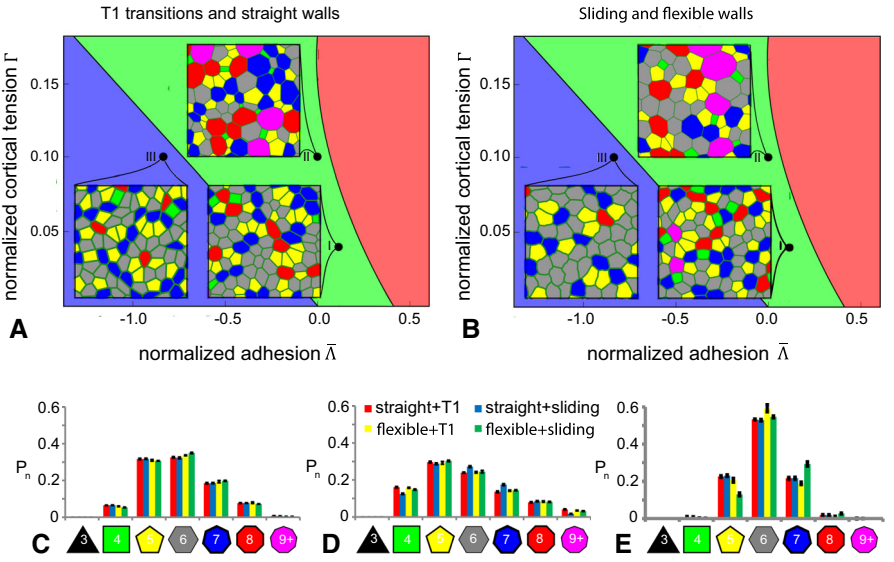

Fig. 4 Comparison of straight walls and T1 transitions with flexible walls and sliding on cell morphology. **a**, **b** Parametric space as in the article of Farhadifar et al. (2007) with three identified morphologies duplicated with VirtualLeaf (cases I, II, and III) at 100.000 MCS. Vertical axis: normalized cortical tension, $\Gamma = \lambda_{\text{cortical}}/(\lambda_A A_T)$; horizontal axis: normalized adhesion, $\overline{\Lambda} = J(\mathbf{e} \to L, \mathbf{e} \to R)/(\lambda_A A_T^{\frac{3}{2}})$. The blue, green, and red regions show the 'ground state' of the vertex model in the absence of cell division for reference (cf. Fig. 1 of Farhadifar et al. 2007): blue, regular hexagonal packing, green: soft networks, red: impossible region. Case I: $\lambda_{\text{cortical}} = 10$, $J(\mathbf{e} \to L, \mathbf{e} \to R) = 500$. Case II: $\lambda_{\text{cortical}} = 26$, $J(\mathbf{e} \to L, \mathbf{e} \to R) = 0$. Case III: $\lambda_{\text{cortical}} = 26$, $J(\mathbf{e} \to L, \mathbf{e} \to R) = -3560$. Hexagonal networks can be found in the green region of the plot. The sum of cortical tension and adhesion energy is smaller than 0 in the blue region, causing a soft network to occur. Simulations within the red region will be unstable. (C, D, E) Relative amounts of cells with n neighbors when the tissue is in equilibrium. C = Case I, D = Case II E = Case III. The bars represent the averages and the error bars the standard deviations of 10 time points between generations 7 and 8. See Supporting Text S1 for detailed simulation descriptions. Bars in C-E are colored in the order red, blue, yellow, green (Color figure online)

to the stochasticity in our simulations, which relaxes the configurations more quickly, similar to the effect of annealing reported in Farhadifar et al. (2007).

3.2.2 Flexible Membranes and Sliding Change Case III, but not Cases I and II

We next tested whether membrane flexibility and the membrane sliding operator could replace algorithm-based T1 transitions to generate a topology indicative of growing tissues. We investigated the performance of these model innovations for three specific cases (Fig. 4b and Videos S11–S13). For Case I and Case II, the simulations in the presence of sliding and membrane flexibility showed no obvious differences with simulations of the vertex model. For Case I (Fig. 4c) and for Case II (Fig. 4d), the distribution of neighbor numbers did not differ between straight membranes (red and blue bars) and flexible membranes (yellow and green bars). Interestingly, for Case III both the visual appearance (Fig. 4b) and the neighbor distribution (Fig. 4e) were strongly affected in the presence of sliding and membrane flexibility (green bars):

The number of heptagons was higher than for the other simulation conditions, and the number of pentagons was reduced. In the absence of membrane flexibility, sliding did not have this effect (blue bars), whereas for membrane flexibility and with T1 transitions, we observed only a small effect (yellow bars).

In Case I and Case II, the line tension (Case I) or cortical tension (Case II) straightens cell boundaries, such that boundary flexibility has no effect. In Case III, the specific topology of 'soft networks' is due to the boundaries' resistance to compression by adjacent cells. Adding additional nodes to the membranes makes them flexible and allows membranes to buckle (see the 'bubbly' boundaries in Fig. 4b and Video S13, Case III), which will likely reduce the number of T1 transitions. We did not understand in detail why the distribution of neighbor numbers was particularly strongly affected in the presence of sliding. A potential explanation is that T1 transitions may introduce spurious energy barriers or time delays between configurations of higher and lower energy, consistent with the incomplete cell sorting discussed in Sect. 3.1.1, whereas for sliding such effects are reduced.

4 Discussion

In this paper, we have introduced extensions of our plant tissue simulation environment VirtualLeaf (Merks et al. 2011; Merks and Guravage 2012), adopting it for the simulation of animal tissues. The key novelty is a method to simulate relative movement of cells, the 'sliding operator.' This operator is applied alongside node displacements in a Metropolis-based energy minimization approach. We have validated the new model using simulations of differential adhesion-driven cell sorting and found that it can reproduce the key phenomena of differential adhesion-driven cell sorting, including cell mixing (Fig. 2a), engulfment of one cell type by the other (Fig. 2b), and cell sorting (Fig. 2c). The extended version of VirtualLeaf also reproduces the key phenomena of epithelial cell packing (Farhadifar et al. 2007) in 'stiff' regimes of the parameter space, i.e., in Cases I and II, where the cell perimeter is under tension ($P(c) > P_T(c)$ and $P_T(c) < 2\sqrt{(\pi A_T(c))}$) (Fig. 4b–d). In the 'soft' parameter regime (Case III), i.e., if the cell perimeter is fully relaxed ($P(c) = P_T(c)$ and $P_T(c) >= 2\sqrt{(\pi A_T(c))}$), the results in VirtualLeaf differ from those reported previously (Farhadifar et al. 2007) due to buckling of the cell–cell interfaces.

The sliding operator requires that cell boundaries are represented by multiple nodes, between which an edge connecting 3 or more cells can 'hop.' Using the sliding operator, topological changes are entirely driven by the energy minimization process through at least two independent moves. In contrast, in traditional VMs, T1 transitions are initiated independently of the energy minimization process, as soon as the length of a cell–cell interface drops below a threshold. Because of this natural integration with the energy minimization algorithm, simulations with the sliding operator more quickly reached complete cell sorting (Fig. 2d) than our simulations with the traditional approach for T1 transitions. A full quantitative comparison of the two approaches will be left for the future work and will give more insight into the causes underlying these differences. For example, lowering the interface length threshold θ_{T1} for the T1 transitions will increase their frequency and will speed up cell sorting for simulations

applying only T1 transitions. Similarly, in simulations applying the new slide operator, increasing the probability of slides and movements by increasing the Boltzmann temperature, T, increases the speed of cell sorting (Fig. 2e). Preliminary simulations with the new slide operator suggest that (perhaps somewhat counterintuitively) increasing the step size has little effect on the speed of cell sorting, because it affects only the node moves, but not the node slides that are responsible for cell rearrangement. Interestingly, our preliminary results suggest that increasing the number of nodes used per cell increases the speed of cell rearrangement (Video S14). A possible reason is that in the refined simulations energy barriers are more easily overcome: The smaller moves are associated with a lower, positive ΔH. A full quantitative analysis of the effect of these and the other parameters on the biological behavior of our model and its computational efficiency will be left to the future work. This analysis will be necessary to decide on the appropriate application domain of this cell-based modeling method among alternative methodology (Osborne et al. 2017). As a first step, we plan to perform detailed comparisons with the CPM, which will require quantitative mapping of the model parameters in VirtualLeaf with those of the CPM. Such quantitative parameter mapping is available for the CPM and VMs (Magno et al. 2015), so these will form an excellent starting point.

Several cases of epithelial sheets have been observed to lack straight boundaries between cells including cells in the *Drosophila* amnioserosa (Toyama et al. 2008; Solon et al. 2009), cells surrounding the closing blastopore in *Xenopus* (Feroze et al. 2015), and the jigsaw puzzle cells of the plant epidermis (Fu et al. 2005; Carter et al. 2017; Sapala et al. 2018). Such irregular boundaries suggest tissue mechanics may be more complex than load-bearing by simple junctional tension (Salbreux et al. 2012). The deviations of cell–cell boundaries from simple lines imply that strain on these structures occurs both parallel and perpendicular to the junction. Deviations may reflect differential pressures between neighboring cells, the ability of the boundary to bend under compression (e.g., Euler buckling), or tensions perpendicular to the boundary. The presence of such irregular boundaries becomes more apparent when imaging tissues with higher magnification or when larger cells are sufficiently resolved by lower magnification objectives. The increasing discovery of such irregular-shaped cells has precipitated several innovations to VMs and related models (Fletcher et al. 2017). Bubbly vertex dynamics (Ishimoto and Morishita 2014) represents the cell–cell and cell–medium interfaces as curves instead of straight lines, where the curvature is due to pressure differences. This innovation changes the forces acting upon the vertices, and hence, it modifies the dynamics of the VM, but it does not allow buckling of cell boundaries. Buckling is possible thanks to our introduction of multiple cell–cell boundary elements between three cell junctions, which parallels similar innovations in VMs and related methods (Tamulonis et al. 2010; Tanaka et al. 2015; Perrone et al. 2016; Fletcher et al. 2017). These adaptations allow simulations of tissues that may experience anisotropic tensions or whose mechanics may be shaped by both medioapical cortical dynamics and junctional contractility. To better simulate such tissues, as a next step we will incorporate a bending stiffness [see, e.g., the bending stiffness of the perimeter in Barton et al. (2017)]. This will make it possible to explore the full parameter range between the maximally stiff, straight cell–cell interfaces

in VMs, and the fully floppy cell–cell interfaces that we can currently represent in VirtualLeaf.

The Hamiltonian and the dynamics of VirtualLeaf (Merks et al. 2011) were inspired by both the Cellular Potts Model (Balter et al. 2007; Merks et al. 2011) and previous vertex-based models of plant tissue morphogenesis (Rudge and Haseloff 2005; Dupuy et al. 2008). The new sliding operator strengthens the similarity of the VirtualLeaf and the CPM, to the extent that our updated VirtualLeaf model can be seen as an 'off-lattice' version of the CPM. A related generalization of the CPM was introduced by Scianna and Preziosi (2016), who have introduced a node-based version of the CPMs. In this generalization, the cells can be represented on any tessellation, which has the advantage that the method can be interfaced with a wider range of methods for continuum mechanics where using arbitrary meshes is useful, e.g., for the finite-element method. The key innovation in their approach, which is shared with VirtualLeaf and VMs, is that cells are represented as polygons. This facilitates simulation of cortical cell tension. Unlike VirtualLeaf or the VM, the cell shapes in node-based CPM are constrained by a tessellation. This possibly introduces similar lattice effects as those found for the CPM, but an advantage of the approach is that it facilitates collision detection. Thus, like the standard CPM, the node-based CPM does not suffer from the limitation of VMs and VirtualLeaf that cell layers must be confluent. Future extensions, e.g., new operators for node fusions in conjunction with efficient collision detection algorithms, will relax those limitations of VirtualLeaf.

In conclusion, with the present extension of a sliding operator, we introduce a new multiparticle method for cell-based modeling and simulation. The method can be categorized within a continuum of closely related multiparticle, Hamiltonian-based methods ranging from lattice-based to off-latice methods. The CPM (Graner and Glazier 1992; Glazier and Graner 1993) is run on a regular lattice. The node-based CPM (Scianna and Preziosi 2016) can be run on irregular lattices. VirtualLeaf takes the CPM 'off the lattice,' with the current restriction that tissues must be confluent. Finally, the VM simplifies the representation of the tissue, by only representing tricellular junctions, connected by straight lines (Weliky and Oster 1990).

References

Anderson ARA, Chaplain MAJ, Rejniak KA (2007) Single-cell-based models in biology and medicine. In: Mathematics and biosciences in interaction. Birkhaüser, Berlin

Antonelli PL, Rogers TD, Willard MA (1973) Geometry and the exchange principle in cell aggregation kinetics. J Theor Biol 41(1):1–21. https://doi.org/10.1016/0022-5193(73)90186-0

Atia L, Bi D, Sharma Y, Mitchel JA, Gweon B, Koehler SA, DeCamp SJ, Lan B, Kim JH, Hirsch R, Pegoraro AF, Lee KH, Starr JR, Weitz DA, Martin AC, Park JA, Butler JP, Fredberg JJ (2018) Geometric constraints during epithelial jamming. Nat Phys 14:613–620. https://doi.org/10.1038/s41567-018-0089-9

Balter A, Merks RMH, Popławski NJ, Swat M, Glazier JA (2007) The Glazier-Graner-Hogeweg model: extensions, future directions, and opportunities for further study. In: Anderson ARA, Rejniak KA (eds) Single cell-based models in biology and medicine. Birkhaüser, Basel, pp 151–167

Barton DL, Henkes S, Weijer CJ, Sknepnek R (2017) Active vertex model for cell-resolution description of epithelial tissue mechanics. PLoS Comput Biol 13(6):e1005569. https://doi.org/10.1371/journal.pcbi.1005569

Belmonte JM, Clendenon SG, Oliveira GM, Swat MH, Greene EV, Jeyaraman S, Glazier JA, Bacallao RL (2016) Virtual-tissue computer simulations define the roles of cell adhesion and proliferation in the onset of kidney cystic disease. Mol Biol Cell 27(22):3673–3685. https://doi.org/10.1091/mbc.E16-01-0059

Bi D, Lopez JH, Schwarz JM, Manning ML (2015) A density-independent rigidity transition inbiological tissues. Nat Phys 11(12):1074–1079. https://doi.org/10.1080/10586458.1992.10504253

Bi D, Yang X, Marchetti MC, Manning ML (2016) Motility-Driven glass and jamming transitions in biological tissues. Phys Rev X. https://doi.org/10.1103/PhysRevX.6.021011

Boas SEM, Merks RMH (2014) Synergy of cell-cell repulsion and vacuolation in a computational model of lumen formation. J R Soc Interface 11(92):20131049–20131049. https://doi.org/10.1038/ncb1705

Boas SEM, Navarro JMI, Merks RMH, Blom JG (2015) A global sensitivity analysis approach for morphogenesis models. BMC Syst Biol 9(1):85. https://doi.org/10.1186/s12918-015-0222-7

Brodland GW (2002) The differential interfacial tension hypothesis (DITH): a comprehensive theory for the self-rearrangement of embryonic cells and tissues. J Biomech Eng Trans ASME 124(2):188. https://doi.org/10.1103/PhysRevLett.76.3032

Brodland GW, Veldhuis JH, Kim S, Perrone M, Mashburn D, Hutson MS (2014) CellFIT: a cellular force-inference toolkit using curvilinear cell boundaries. PLoS One 9(6):e99116. https://doi.org/10.1371/journal.pone.0099116

Carmona-Fontaine C, Matthews HK, Kuriyama S, Moreno M, Dunn GA, Parsons M, Stern CD, Mayor R (2008) Contact inhibition of locomotion in vivo controls neural crest directional migration. Nature 456(7224):957–961. https://doi.org/10.1038/nature07441

Carter R, Sánchez-Corrales YE, Hartley M, Grieneisen VA, Marée AFM (2017) Pavement cells and the topology puzzle. Development (Cambridge, England) 144(23):4386–4397. https://doi.org/10.1242/dev.157073

De Vos D, Dzhurakhalov A, Stijven S, Klosiewicz P, Beemster GTS, Broeckhove J (2017) Virtual plant tissue: building blocks for next-generation plant growth simulation. Front Plant Sci 8:686. https://doi.org/10.3389/fpls.2017.00686

Dupuy L, Mackenzie J, Rudge T, Haseloff J (2008) A system for modelling cell-cell interactions during plant morphogenesis. Ann Bot 101(8):1255–1265. https://doi.org/10.1093/aob/mcm235

Farhadifar R, Röper JC, Aigouy B, Eaton S, Jülicher F (2007) The influence of cell mechanics, cell-cell interactions, and proliferation on epithelial packing. Curr Biol 17(24):2095–2104. https://doi.org/10.1016/j.cub.2007.11.049

Feroze R, Shawky JH, von Dassow M, Davidson LA (2015) Mechanics of blastopore closure during amphibian gastrulation. Dev Biol 398(1):57–67. https://doi.org/10.1016/j.ydbio.2014.11.011

Fletcher AG, Cooper F, Baker RE (2017) Mechanocellular models of epithelial morphogenesis. Philos Trans R Soc B Biol Sci 372(1720):20150519. https://doi.org/10.1098/rstb.2015.0519

Fu Y, Gu Y, Zheng Z, Wasteneys G, Yang Z (2005) Arabidopsis interdigitating cell growth requires two antagonistic pathways with opposing action on cell morphogenesis. Cell 120(5):687–700. https://doi.org/10.1016/j.cell.2004.12.026

Ghaffarizadeh A, Heiland R, Friedman SH, Mumenthaler SM, Macklin P (2018) PhysiCell: an open source physics-based cell simulator for 3-D multicellular systems. PLoS Comput Biol 14(2):e1005991. https://doi.org/10.1371/journal.pcbi.1005991

Gibson MC, Patel AB, Nagpal R, Perrimon N (2006) The emergence of geometric order in proliferating metazoan epithelia. Nature 442(7106):1038–1041. https://doi.org/10.1038/nature05014

Glazier JA, Graner F (1993) Simulation of the differential adhesion driven rearrangement of biological cells. Phys Rev E 47(3):2128–2154

Graner F, Glazier JA (1992) Simulation of biological cell sorting using a two-dimensional extended Potts model. Phys Rev Lett 69(13):2013–2016

Graner F, Sawada Y (1993) Can surface adhesion drive cell rearrangement? J Theor Biol 164:477–506

Harris AK (1976) Is cell sorting caused by differences in the work of intercellular adhesion? A critique of the Steinberg hypothesis. J Theor Biol 61(2):267–285. https://doi.org/10.1016/0022-5193(76)90019-9

Hester SD, Belmonte JM, Gens JS, Clendenon SG, Glazier JA (2011) A multi-cell, multi-scale model of vertebrate segmentation and somite formation. PLoS Comput Biol 7(10):e1002155

Honda H, Dan-Sohkawa M, Watanabe K (1983) Geometrical analysis of cells becoming organized into a tensile sheet, the blastular wall, in the starfish. Differentiation 25(1–3):16–22. https://doi.org/10.1111/j.1432-0436.1984.tb01332.x

Hutson MS, Brodland GW, Yang J, Viens D (2008) Cell sorting in three dimensions: topology, fluctuations, and fluidlike instabilities. Phys Rev Lett 101(14):4

Ishimoto Y, Morishita Y (2014) Bubbly vertex dynamics: a dynamical and geometrical model for epithelial tissues with curved cell shapes. Phys Rev E 90(5–1):052711. https://doi.org/10.1103/PhysRevE.90.052711

Keller EF, Segel LA (1970) Initiation of slime mold aggregation viewed as an instability. J Theor Biol 26(3):399–415

Keller EF, Segel LA (1971) Model for chemotaxis. J Theor Biol 30(2):225–234. https://doi.org/10.1016/0022-5193(71)90050-6

Kim S, Cai M, Hilgenfeldt S (2014) Lewis' law revisited: the role of anisotropy in size-topology correlations. New J Phys 16(1):015024. https://doi.org/10.1088/1367-2630/16/1/015024

Krieg MM, Arboleda-Estudillo YY, Puech PHP, Käfer JJ, Graner FF, Müller DJD, Heisenberg CPC (2008) Tensile forces govern germ-layer organization in zebrafish. Nat Cell Biol 10(4):429–436

Kudryashova N, Tsvelaya V, Agladze K, Panfilov A (2017) Virtual cardiac monolayers for electrical wave propagation. Sci Rep 7(1):7887. https://doi.org/10.1038/s41598-017-07653-3

Lander AD (2007) Morpheus unbound: reimagining the morphogen gradient. Cell 128(2):245–256. https://doi.org/10.1016/j.cell.2007.01.004

Lewis FT (1926) The effect of cell division on the shape and size of hexagonal cells. Anat Rec 33(5):331–355. https://doi.org/10.1002/ar.1090330502

Liedekerke P, Palm MM, Jagiella N, Drasdo D (2015) Simulating tissue mechanics with agent-based models: concepts, perspectives and some novel results. Comput Part Mech 2(4):401–444. https://doi.org/10.1007/s40571-015-0082-3

Magno R, Grieneisen VA, Marée AF (2015) The biophysical nature of cells: potential cell behaviours revealed by analytical and computational studies of cell surface mechanics. BMC Biophys 8(1):2038. https://doi.org/10.1186/s13628-015-0022-x

Maree A, Hogeweg P (2002) Modelling dictyostelium discoideum morphogenesis: the culmination. Bull Math Biol 64(2):327–353. https://doi.org/10.1006/bulm.2001.0277

Merkel M, Manning ML (2017) Using cell deformation and motion to predict forces and collective behavior in morphogenesis. Semin Cell Dev Biol 67:161–169. https://doi.org/10.1016/j.semcdb.2016.07.029

Merks R (2015) Cell-based modeling. In: Engquist B (ed) Encyclopedia of applied and computational mathematics. Springer, Berlin, pp 195–201. https://doi.org/10.1007/978-3-540-70529-1_70

Merks RMH, Brodsky SV, Goligorksy MS, Newman SA, Glazier JA (2006) Cell elongation is key to in silico replication of in vitro vasculogenesis and subsequent remodeling. Dev Biol 289(1):44–54. https://doi.org/10.1016/j.ydbio.2005.10.003

Merks RMH, Glazier JA (2005) A cell-centered approach to developmental biology. Physica A 352(1):113–130

Merks RMH, Guravage M, Inzé D, Beemster GTS (2011) VirtualLeaf: an open-source framework for cell-based modeling of plant tissue growth and development. Plant Phys 155(2):656–666. https://doi.org/10.1104/pp.110.167619

Merks RMH, Guravage M, Inze D, Beemster GTS (2011) VirtualLeaf: an open-source framework for cell-based modeling of plant tissue growth and development. Plant Physiol 155(2):656–666

Merks RMH, Guravage MA (2012) Building simulation models of developing plant organs using VirtualLeaf. In: De Smet I (ed) Plant organogenesis: methods and protocols. Methods in molecular biology. Springer, New York, pp 333–352. https://doi.org/10.1007/978-1-62703-221-6_23

Newman T (2005) Modeling multicellular systems using subcellular elements. Math Biosci Eng 2(3):613–624

Odell GM, Oster G, Alberch P, Burnside B (1981) The mechanical basis of morphogenesis. I. Epithelial folding and invagination. Dev Biol 85(2):446–462

Osborne JM, Fletcher AG, Pitt-Francis JM, Maini PK, Gavaghan DJ (2017) Comparing individual-based approaches to modelling the self-organization of multicellular tissues. PLoS Comput Biol 13(2):e1005387. https://doi.org/10.1371/journal.pcbi.1005387.s004

Painter KJ, Bloomfield JM, Sherratt JA, Gerisch A (2015) A nonlocal model for contact attraction and repulsion in heterogeneous cell populations. Bull Math Biol 77(6):1132–1165. https://doi.org/10.1007/s11538-015-0080-x

Palachanis D, Szabó A, Merks RMH (2015) Particle-based simulation of ellipse-shaped particle aggregation as a model for vascular network formation. Comput Part Mech 2(4):371–379. https://doi.org/10.1007/s40571-015-0064-5

Palm MM, Dallinga MG, van Dijk E, Klaassen I, Schlingemann RO, Merks RMH (2016) Computational screening of tip and stalk cell behavior proposes a role for apelin signaling in sprout progression. PLoS One 11(11):e0159478. https://doi.org/10.1371/journal.pone.0159478.s016

Perrone MC, Veldhuis JH, Brodland GW (2016) Non-straight cell edges are important to invasion and engulfment as demonstrated by cell mechanics model. Biomech Model Mechanobiol 15(2):405–418. https://doi.org/10.1007/s10237-015-0697-6

Rudge T, Haseloff J (2005) A computational model of cellular morphogenesis in plants. Lect Notes Comput Sci 3630:78–87

Sahlin P, Jönsson H (2010) A modeling study on how cell division affects properties of epithelial tissues under isotropic growth. PLoS One 5(7):e11750. https://doi.org/10.1371/journal.pone.0011750.t002

Salbreux G, Charras G, Paluch E (2012) Actin cortex mechanics and cellular morphogenesis. Trends Cell Biol 22(10):536–545. https://doi.org/10.1016/j.tcb.2012.07.001

Sapala A, Runions A, Routier-Kierzkowska AL, Das Gupta M, Hong L, Hofhuis H, Verger S, Mosca G, Li CB, Hay A, Hamant O, Roeder AH, Tsiantis M, Prusinkiewicz P, Smith RS (2018) Why plants make puzzle cells, and how their shape emerges. eLife 7:e32794. https://doi.org/10.7554/eLife.32794

Scianna M, Preziosi L (2016) A node-based version of the cellular Potts model. Comput Biol Med 76:94–112. https://doi.org/10.1016/j.compbiomed.2016.06.027

Sluka JP, Fu X, Maaciej S, Belmonte JM, Cosmanescu A, Clendenon SG, Wambaugh JF, Glazier JA (2016) A liver-centric multiscale modeling framework for xenobiotics. PLoS One 11(9):e0162428. https://doi.org/10.1371/journal.pone.0162428.s005

Smeets B, Alert R, Pešek J, Pagonabarraga I, Ramon H, Vincent R (2016) Emergent structures and dynamics of cell colonies by contact inhibition of locomotion. Proc Natl Acad Sci USA 113(51):14621–14626. https://doi.org/10.1073/pnas.1521151113

Solon J, Kaya-Copur A, Colombelli J, Brunner D (2009) Pulsed forces timed by a ratchet-like mechanism drive directed tissue movement during dorsal closure. Cell 137(7):1331–1342. https://doi.org/10.1016/j.cell.2009.03.050

Sozinova O, Jiang Y, Kaiser D, Alber M (2006) A three-dimensional model of myxobacterial fruiting-body formation. Proc Natl Acad Sci USA 103(46):17255–17259. https://doi.org/10.1073/pnas.0605555103

Staple DB, Farhadifar R, Röper JC, Aigouy B, Eaton S, Jülicher F (2010) Mechanics and remodelling of cell packings in epithelia. Eur Phys J E 33(2):117–127. https://doi.org/10.1007/s004540010071

Steinberg M (1963) Reconstruction of tissues by dissociated cells. Science (New York, NY) 141:401–408

Steinberg MS (1996) Adhesion in development: an historical overview. Dev Biol 180(2):377–388. https://doi.org/10.1006/dbio.1996.0312

Steinberg MS (2007) Differential adhesion in morphogenesis: a modern view. Curr Opin Genet Dev 17(4):281–286. https://doi.org/10.1016/j.gde.2007.05.002

Sulsky D, Childress S, Percus JK (1984) A model of cell sorting. J Theor Biol 106(3):275–301

Tamulonis C, Postma M, Marlow HQ, Magie CR, de Jong J, Kaandorp J (2010) A cell-based model of Nematostella vectensis gastrulation including bottle cell formation, invagination and zippering. Dev Biol 351(1):217–228. https://doi.org/10.1016/j.ydbio.2010.10.017

Tanaka S, Sichau D, Iber D (2015) LBIBCell: a cell-based simulation environment for morphogenetic problems. Bioinformatics (Oxford, England) 31(14):2340–2347. https://doi.org/10.1093/bioinformatics/btv147

Tlili S, Gauquelin E, Li B, Cardoso O, Ladoux B, Delanoë-Ayari H, Graner F (2018) Collective cell migration without proliferation: density determines cell velocity and wave velocity. R Soc Open Sci 5:172421. https://doi.org/10.1098/rsos.172421

Toyama Y, Peralta XG, Wells AR, Kiehart DP, Edwards GS (2008) Apoptotic force and tissue dynamics during Drosophila embryogenesis. Science (New York, NY) 321(5896):1683–1686. https://doi.org/10.1126/science.1157052

Voss-Böhme A, Deutsch A (2010) The cellular basis of cell sorting kinetics. J Theor Biol 263(4):419–436. https://doi.org/10.1016/j.jtbi.2009.12.011

Weliky M, Oster G (1990) The mechanical basis of cell rearrangement. I. Epithelial morphogenesis during Fundulus epiboly. Development (Cambridge, England) 109(2):373–386

Woods ML, Carmona-Fontaine C, Barnes CP, Couzin ID, Mayor R, Page KM (2014) Directional collective cell migration emerges as a property of cell interactions. PLoS One 9(9):e104969. https://doi.org/10.1371/journal.pone.0104969.s012

Affiliations

Henri B. Wolff[1,2,3] · Lance A. Davidson[2] · Roeland M. H. Merks[1,4,5]

✉ Lance A. Davidson
lad43@pitt.edu

✉ Roeland M. H. Merks
merksrmh@math.leidenuniv.nl

1 Centrum Wiskunde and Informatica, Science Park 123, 1098 XG Amsterdam, The Netherlands

2 Departments of Bioengineering, Developmental Biology, and Computational and Systems Biology, University of Pittsburgh, Bioscience Tower 3-5059 3501 Fifth Avenue, Pittsburgh, PA, USA

3 Present Address: Department of Epidemiology and Biostatistics, Decision Modeling Center VUmc, Amsterdam UMC location VUmc, PO Box 7057, 1007 MB Amsterdam, The Netherlands

4 Mathematical Institute, University Leiden, P.O. Box 9512, 2300 RA Leiden, The Netherlands

5 Present Address: Mathematical Institute and Institute of Biology, Leiden University, P.O. Box 9505, 2300 RA Leiden, The Netherlands